Influence of M-Phase Chromatin on the Anisotropy of Microtubule Asters

M. Dogterom, M.-A. Félix, C.C. Guet, and S. Leibler

Departments of Physics and Molecular Biology, Princeton University, Princeton, New Jersey 08544

Abstract. In many eukaryotic cells going through M-phase, a bipolar spindle is formed by microtubules nucleated from centrosomes. These microtubules, in addition to being "captured" by kinetochores, may be stabilized by chromatin in two different ways: short-range stabilization effects may affect microtubules in close contact with the chromatin, while long-range stabilization effects may "guide" microtubule growth towards the chromatin (e.g., by introducing a diffusive gradient of an enzymatic activity that affects microtubule assembly). Here, we use both meiotic and mitotic extracts from *Xenopus laevis* eggs to study microtubule aster formation and microtubule dynamics in the presence of chromatin. In "low-speed" meiotic extracts, in the presence of salmon sperm chromatin, we find that short-range stabilization effects lead to a strong anisotropy of the microtubule asters. Analysis of the dy-

namic parameters of microtubule growth shows that this anisotropy arises from a decrease in the catastrophe frequency, an increase in the rescue frequency and a decrease in the growth velocity. In this system we also find evidence for long-range "guidance" effects, which lead to a weak anisotropy of the asters. Statistically relevant results on these long-range effects are obtained in "high-speed" mitotic extracts in the presence of artificially constructed chromatin stripes. We find that aster anisotropy is biased in the direction of the chromatin and that the catastrophe frequency is reduced in its vicinity. In this system we also find a surprising dependence of the catastrophe and the rescue frequencies on the length of microtubules nucleated from centrosomes: the catastrophe frequency increases and the rescue frequency decreases with microtubule length.

T HE role of mitosis and meiosis is to spatially distribute chromosomes between two daughter cells. This process is accomplished by the bipolar spindle, a complex molecular system made of microtubules (MTs)[1] and associated proteins (McIntosh and Koonce, 1989; Karsenti, 1991). An important problem in the study of cell division is the origin of bipolar symmetry of the spindle. In many cases MTs are nucleated by a microtubule organizing center such as a centrosome. Duplicated centrosomes separate at the onset of spindle formation and two MT "asters" are formed. In prometaphase these two MT asters become anisotropic and the density and/or the length of

MTs become biased towards the center plane around which the chromosomes accumulate. Although it is clear that the anisotropy of the asters arises mainly as a consequence of interactions between MTs and chromosomes, the detailed mechanism is not yet fully understood.

In one scenario, centrosome-nucleated MTs that assemble through the out-of-equilibrium process of dynamic instability (Mitchison and Kirschner, 1984*a,b*) perform a random "search" in space for their targets (Holy and Leibler, 1994), which are the chromosomes, or more precisely the kinetochores. The anisotropy of each aster, and thus the bipolar symmetry of the spindle, arrives as a simple consequence of the selective stabilization or "capture" of MTs by the kinetochores (Kirschner and Mitchison, 1986). There is a growing body of evidence that this scenario is not the only possible assembly pathway for a bipolar spindle (Rieder et al., 1993). In many meiotic systems, such as in some insect spermatocytes (Church et al., 1986; Steffen et al., 1986) and oocytes (Karsenti et al., 1984; Theurkauf and Hawley, 1992), the chromosomes themselves seem to promote the assembly of MTs in their vicinity, which then organize into a bipolar spindle in a process that does not require the presence of separate nucleation centers (e.g., centrosomes) (Pickett-Heaps et al., 1982;

1. *Abbreviations used in this paper:* MAP, microtubule-associated protein; MTs, microtubules.

Nicklas, 1988). Also, in *Xenopus* egg extracts bipolar spindles form around meiotic chromatin in the absence of kinetochores (Sawin and Mitchison, 1991), and in grasshopper spermatocytes MT polymerization seems to be enhanced by chromatin in a way that is independent of the number of kinetochores present (Zhang and Nicklas, 1995). These experimental observations suggest that chromatin may be more actively involved in the regulation of MT assembly and spindle formation than it is suggested by the first scenario described above, in which kinetochores are purely passive targets waiting to be "hit" by randomly assembling MTs.

In this paper we explore further this possibility. In particular, we evaluate quantitatively the influence of chromatin on the dynamical assembly and stabilization of MTs nucleated at the centrosome. It has been proposed that the role of chromatin may be twofold. First, it may stabilize MTs when they move into its immediate vicinity or come into direct physical contact as observed, for instance, in vitro (Sawin and Mitchison, 1991). Second, it may guide the MTs during their search for kinetochores, for example by introducing a gradient of a diffusible biochemical signal that affects MT assembly. To effects observed in the absence of physical contact between MTs and the chromatin we will refer as long-range stabilization (or "guidance") effects. Any effects observed in close contact with the chromatin will be called short-range stabilization effects. It should be noted that the latter may result from direct physical contact and/or the presence of a diffusible biochemical signal, whereas long-range effects cannot be explained by direct interaction between MTs and the chromatin.

Cell-free *Xenopus laevis* egg extracts can be prepared in defined cell cycle states (Lohka and Masui, 1983; Murray and Hunt, 1993) and then be used to study cellular events under mitotic control, such as MT assembly and spindle formation (Gard and Kirschner, 1987; Belmont et al., 1990; Verde et al., 1990, 1992; Sawin and Mitchison, 1991). Here, we introduce chromatin into *Xenopus* egg extracts to study its influence on the assembly of MT asters nucleated by separately added centrosomes. Since we are not interested here in stabilization of MTs by kinetochores, we introduce the chromatin into our systems in such a way that kinetochores are absent and/or may be completely neglected.

First, by adding centrosomes and large quantities of salmon sperm nuclei to "low-speed" meiotic extracts (10,000-*g* supernatant), we are able to observe the growth of MT asters in the vicinity of randomly distributed chromatin. The low density of MTs in these assays allows us to quantitate the dynamics of individual MTs, using video-enhanced fluorescence microscopy. In experiments with high-speed mitotic extracts (100,000-*g* supernatant), which are more homogeneous than the low-speed extracts, we form a pattern of chromatin built from (λ-phage) DNA molecules attached in a controlled way to a glass surface. The precise control of the geometry of the chromatin allows us to reproduce many times the measurement of MT dynamics in asters placed in a similar fashion with respect to chromatin and thus obtain statistically significant results. In both experiments we search for short-range and long-range stabilization effects of chromatin on centrosome-nucleated MTs.

Materials and Methods

Materials

Chemicals, as well as salmon sperm nuclei, were purchased from Sigma Chemical Co. (St. Louis, MO) unless noted otherwise. Centrosomes were obtained from T. Mitchison or prepared in our lab according to (Mitchison and Kirschner, 1986) (stock concentration: $\sim 10^7$/ml). Plasmid for the expression of sea urchin Δ90 cyclin B was obtained from T. Mitchison and M. Glotzer (University of California, San Francisco). The protein was expressed in *Escherichia coli* and purified according to Glotzer et al. (1991) (final protein concentration: 0.4 mg/ml). Tubulin was purified from bovine brain according to Mitchison and Kirschner (1984b) and labeled according to Hyman et al. (1991) with tetramethylrhodamine succinimidyl ester (C-1171; Molecular Probes, Eugene, OR) (final protein concentration: 22 mg/ml). The stoichiometry of labeling was estimated to be 1.5 rhodamines per tubulin dimer.

Frog Eggs and Egg Extracts

Xenopus laevis females were prepared and induced to lay eggs as previously described (Verde et al., 1992). Meiotic, low-speed extracts were prepared from unfertilized eggs according to Murray (1991) with some modifications. After collection of the eggs, the jelly coat was removed with 2.5% (wt/vol) L-cysteine in 100 mM KCl, 2mM MgCl₂, pH 7.8. Eggs were washed in modified extract buffer (MXB; 100 mM KCl, 2mM MgCl₂, 10 mM K-Hepes, 50 mM sucrose, 10 mM EGTA, pH 7.7). They were packed by a brief centrifugation (300 *g*, 15°C) in MXB containing 10 μg/ml leupeptin, 10 μg/ml aprotinin, 10 μg/ml pepstatin, and 5 μg/ml cytochalasin D. Excess buffer was removed and the eggs were crushed by centrifugation at 10,000 *g* (15 min, 15°C). An ATP regenerating system (final concentration: 1 mM ATP, 10 mM creatine phosphate, 80 μg/ml creatine phosphokinase) was added and 50-μl aliquots were frozen and stored in liquid nitrogen. The extracts were tested for their ability to form half-spindles in the presence of demembranated *Xenopus* sperm nuclei (as reported by Sawin and Mitchison, 1991).

Mitotic, high-speed extracts were prepared exactly as described previously (Verde et al., 1992). Aliquots of interphase arrested extract (50 μl) were frozen and stored in liquid nitrogen. Before use, these extracts were driven into a mitotic(-like) state by the addition of 1/20 vol of Δ90 cyclin B. This caused the endogenous cdc2 kinase activity to increase from 4 to 25 pmol/min/μl in 20 min as measured by the histone H1 kinase activity. The histone H1 kinase activity was measured according to Félix et al. (1989) on histone H1 type III-S.

Binding DNA to Gold Stripes

Biotinylated DNA molecules from λ-phage were linked with streptavidin to biotinylated gold stripes patterned on glass coverslips according to Zimmermann and Cox (1993) (see Fig. 1).

DNA and enzymes were purchased from New England Biolabs (Beverly, MA) and nucleotides from Boehringer Mannheim Corp. (Indianapolis, IN). Long double-stranded DNA molecules were obtained by ligating λ-DNA using T4 DNA ligase. λ-DNA at 450 μg/ml in ligase buffer was incubated with ligase (1450 U/ml) at room temperature for 1 h. The ligase was inactivated by incubation at 65°C for 10 min. The DNA molecules were labeled on one end with biotin by partially filling in the recessed ends using the Klenow fragment of T4 polymerase. Ligated λ-DNA molecules at 100 μg/ml were incubated in polymerase buffer with polymerase (5 U/ml), dATP, dGTP (both 400 μM), and biotin-16-dUTP (4 μM) for 1 h at 36°C (dCTP was missing from this reaction to ensure one-sided labeling of the DNA molecules). Biotinylated DNA was separated from free biotin by replacing the solvent seven times with TE buffer (100 mM Tris-HCl, 1 mM EDTA, pH 8.0) using a spin filter (Centricon 30; Amicon, Beverly, MA) and stored in TE buffer at −20°C at a concentration of 200 μg/ml.

Glass coverslips (no. 1, 22 × 22 mm) were cleaned for 1 h in a mixture of water, hydrogen peroxide and ammonium hydroxide (5:1:1 by volume) at 70°C, rinsed several times with distilled/deionized water and dried in a heated vacuum chamber. They were patterned with 150 nm thick, 100-μm-wide gold stripes (separated by 500 μm) using standard photolithography and vapor deposition techniques (Fig. 1, steps I–IV) (a thin layer of chromium was deposited prior to the gold to serve as an adhesion layer). They were cleaned once more as described above and either used directly or stored in water for up to one week.
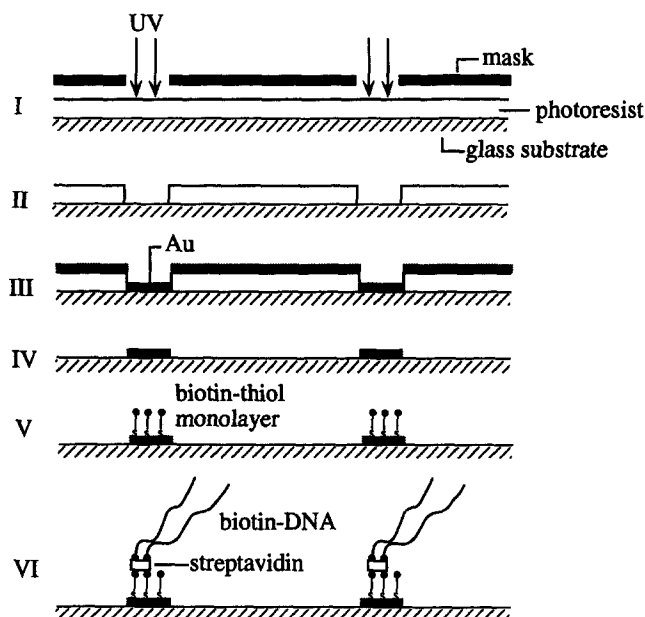
Figure 1. Procedure for binding DNA to gold stripes (schematic drawing, not to scale). Step I: A glass substrate (coverslip) was covered with photoresist and exposed to UV light using a mask. The mask was made of a piece of slide film showing a pattern of 100-μm-wide white lines, separated by 500 μm on a black background. Step II: The photoresist was developed, which cleared 100-μm-wide lines on the glass. Step III: A thin layer (150 nm) of gold (Au) was deposited on the cleared glass. Step IV: The remaining photoresist was removed. Step V: A monolayer of thiol groups linked to biotin molecules was assembled on the gold lines. Step VI: Using streptavidin as a linker, biotinylated DNA was attached to the biotinylated stripes.

The gold stripes were biotinylated by assembling a monolayer of thiol groups linked to biotin molecules on their surface (Fig. 1, step V). A solution of 5 mg/ml biotin-HPDP (Pierce Chem. Co., Rockford, IL) in DMF (stored in 20-μl aliquots at −80°C) was incubated for 5 min with 1/20 vol of tri-*n*-butylphosphine, a reducing agent. The reduced solution contained a mixture of biotin-HP-thiol and pyridine thiol. The patterned surfaces were rinsed with a water/methanol (1:1) solution and incubated for 10 min on 200 μl (placed as a drop on a piece of parafilm) of the biotin-HP-thiol solution diluted 20 times in water/methanol (1:1). They were then rinsed

in water/methanol (1:1), rinsed in PB (0.1 M phosphate buffer, pH 7.0) and incubated for 30 min on 100 μl streptavidin (0.2 mg/ml in PB). Finally the surfaces were rinsed in TE, incubated for 2 h on 100 μl biotinylated DNA (20 μg/ml in TE), rinsed again in TE, and then used immediately. Using techniques involving restriction enzymes or radiolabeling of the DNA, we estimated the final surface density of DNA to be on the order of 0.02 μg/cm², while undetectable amounts of DNA bound to the glass in between gold stripes (data not shown). In addition, visual inspection of many DNA-coated gold stripes revealed high contrast in DNA binding between gold and glass surfaces, and high homogeneity in binding to gold surfaces (see Fig. 6, *inset*). For control experiments in the absence of chromatin only the final incubation with DNA was omitted.

Sample Preparation for Video Microscopy

Meiotic low-speed extracts were mixed with rhodamine-labeled tubulin (final 0.22 mg/ml), the DNA dye YO-PRO-1 (Molecular Probes, Inc., Eugene, OR; final 0.5 μM), and 2 μm (diameter) latex fluorescent beads used as spacers (Duke Scientific Corp., Palo Alto, CA; final ~10⁷/ml), and were kept on ice for up to 1 h. A solution of 10–20 mg/ml salmon sperm nuclei (Sigma S-3126) was prepared freshly in 5 mM K-Pipes, 0.5 mM EDTA, 5 mM MgCl₂, 5 mM NaCl, pH 7.2. The extract was incubated with 1/20 vol of this solution for 30 min at room temperature (final concentration: ~10⁴ nuclei/μl) and for another 10 min with 1/20 vol of centrosomes. Finally an oxygen scavenger system as in Verde et al. (1992) and 1/20 vol of a freshly prepared, saturated solution of hemoglobin in water were added (we find that this combination gives the best results against photobleaching effects). 1.5–2 μl of extract were squashed under a 22 × 22 mm ethanol-cleaned coverslip, and the sample was sealed with melted paraffin. Several such samples were prepared simultaneously and either observed immediately or kept at 4°C until observation (within 1 h).

Gold-patterned coverslips with (or without) DNA were washed in acetate buffer (excess buffer was removed by blotting the coverslip on one side with a Kimwipe) and incubated on 50 μl high-speed extract in the presence of Δ90 cyclin B for 1 h (all coverslip incubations were performed on a piece of parafilm at room temperature). This incubation allowed the DNA to assemble histones and other proteins from the extract and form mitotic chromatin (Hirano and Mitchison, 1991). Starting 30 min later, a fresh 50-μl aliquot of extract was incubated with cyclin B; another 30 min later rhodamine tubulin (final 0.22 mg/ml), YO-PRO-1 (final 1 μM), beads (final ~10⁷/ml), and 1/40 vol of hemoglobin (see above) were added. 40 μl of this mixture was used to wash the preincubated coverslip. To the remaining 10-μl sample we added 1/10 vol of centrosomes and the oxygen scavenger system (see above). A drop of 8 μl was placed immediately on a second, larger (24 × 60 mm) ethanol-cleaned coverslip. The preincubated coverslip was placed on this drop, pressed down firmly and excess fluid was blotted away from the sides. The sample was finally sealed with paraffin. To examine the DNA stripes without incubation on the extract, they were briefly incubated on TE with 1 μM YO-PRO-1, positioned on a second (large) coverslip and sealed with paraffin.

SALMON SPERM

Vary Θ to maximize anisotropy
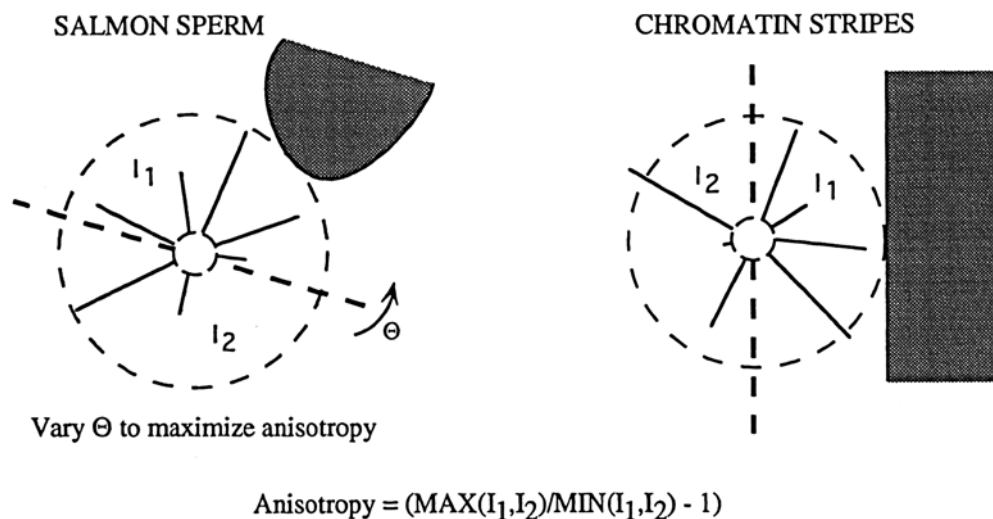
CHROMATIN STRIPES

Figure 2. Schematic drawing showing the method we use to measure the aster anisotropy in the experiments with salmon sperm chromatin and in the experiments with artificial chromatin stripes (chromatin regions in gray). I_1 and I_2 are the integrated and time-averaged fluorescence intensities produced by MTs on opposite sides of the centrosome. The anisotropy is calculated from these intensities using the formula given.

$$\text{Anisotropy} = (\text{MAX}(I_1,I_2)/\text{MIN}(I_1,I_2) - 1)$$

Video Microscopy/Data Acquisition

Time lapse recordings of MT asters were made using a Zeiss inverted microscope (Axiovert 135) set up for epifluorescence, equipped with a Mercury 100W illuminator, a standard filter set for rhodamine, a 63× Plan Apochromat objective (oil immersed; N.A. 1.4), a 1.6× optovar lens (optional) and a 4× extra magnification lens attached to a camera port at the bottom of the microscope (the Keller hole). A neutral density filter (50%) in the illumination pathway was used to reduce photobleaching effects. Images were collected using an intensified high resolution CCD camera (Paultek Corp., Grass Valley, CA), an OMNEX image processor (Imagen Instrumentation Inc., Trenton, NJ) and a Pixelbuffer framegrabber card (Perceptics Corp., Knoxville, TN) on a Macintosh Quadra 900 Computer. Using an electronic timer (JML Optical, Rochester, NY), a shutter (JML Optical) placed between the illuminator and the microscope was triggered to open every 2 s for a 0.27-s interval. The same trigger was used to drive software written with NIH Image, to save an eight-frame averaged image to a hard drive at the end of each interval. Up to 200 consecutive images were recorded for each individual aster (which corresponds to ~7 min in real time). For storage, the digitized images were downloaded to a DAT tape using a DAT drive (Hewlett Packard, Palo Alto, CA) and Retrospect software (Dantz Development Corp., Orinda, CA). After each run we switched the filter set to a standard set for FITC (used for YO-PRO-1) and stored a snapshot of the DNA using the same equipment. Pseudo-color images were made on a SGI (Silicon Graphics, Mountain View, CA) computer, superimposing two black-and-white images after converting them to colored images (MT asters to green and DNA to red).

Measuring Anisotropy in Fluorescence Intensity

The anisotropy in fluorescence intensity produced by MT asters was measured in the following way (see schematic drawing in Fig. 2): for each aster an axis through, and a maximum radius around the centrosome were defined. In the experiments with the salmon sperm, the direction (or angle Θ) of the axis was varied and afterwards selected to maximize the anisotropy. In the experiments with the chromatin stripes, the axis was chosen parallel to the glass/gold interface. The position of the axis had to be redefined slightly for each frame to account for small changes in the position of the aster. The maximum radius around the centrosome was defined by the size of the aster, the minimum distance of the center of the centrosome to the edge of the image or the minimum distance of the centrosome to the chromatin structure, whichever was the smallest. The high density of MTs in the center of the aster in general caused saturation of the pixel brightness in a small area around the centrosome. This blurred area was eliminated by defining also a minimum radius around the centrosome (typically 2–3 μm). Using a home written computer program, the intensity of all pixels above a certain grayscale (chosen to select for MTs and to eliminate, as much as possible, pixels that were only contributing to the background) was integrated in the two thus defined areas on either side of the centrosome. The results were averaged over all images in the time sequence of that particular aster, the ratio of these two integrated intensities (Fig. 2, I_1 and I_2) was calculated and the amount by which this ratio exceeds 1 was used as a measure of anisotropy. In the experiments with salmon sperm chromatin, the vector perpendicular to the axis that produces the highest anisotropy, which points in the direction of highest fluorescence, is called the maximum anisotropy vector. We discarded sequences of images in which there was obvious fluid flow, too many small free MTs in the field of view, or very poor image contrast.

Measuring the Dynamic Parameters

The parameters of dynamic instability were measured essentially as described in Verde et al. (1992), with the exception that the growth and shrinkage velocities were calculated by averaging the MT length changes over 2-s intervals. Examples of typical MT length traces obtained in meiotic and mitotic extracts are shown in Fig 4.

In the experiments with meiotic extracts and salmon sperm chromatin the dynamic parameters were measured for each individual aster. The images were divided in two half planes by an axis running through the center of the aster perpendicular to the direction of the chromatin. The chromatin was defined to be localized at the point where the chromatin-centrosome distance is the smallest. Note that the axis chosen to be perpendicular to the direction of the chromatin is not necessarily the same as the axis of highest anisotropy discussed above (see Fig. 2). The dynamic parameters were calculated as described above on either side of this axis, leaving out the area within a 5-μm radius around the center of the aster

(MTs smaller than 5 μm were not taken into account because they were often overlapping and easily confused with each other). In each half plane typically 15–25 MTs were tracked for a total time of 20–25 min, and on the order of 10–20 catastrophe and 0–5 rescue events were counted (only in Fig. 3 *a* more rescues were counted).

In the experiments with mitotic extracts and chromatin stripes the data from all asters recorded in the presence or in the absence of chromatin were combined. All data from asters that were recorded between 30 and 65 min after finishing the sample preparation were used. Data taken during the initial 30 min were discarded, because initial fluid flow was often observed, and because we found that the dynamic parameters varied with time during this period (data not shown). In the presence (absence) of chromatin, a total of 13,375 (7,455) growth events (a total of 446 [249] min), 5,655 (3,936) shrinkage events (a total of 189 [131] min), 607 (436) catastrophe events, and 240 (98) rescue events were counted (see Fig. 8). The dynamic parameters were calculated as described above either as a function of MT length or as a function of the distance to the gold stripe, i.e., events were counted either in 2-μm-wide rings centered around the centrosome or in 5-μm-wide bands parallel to the edge of the gold stripe. Events for MTs shorter than 3 μm or longer than 15 μm were not taken into account (because such MTs were hard to follow and/or were rare). To normalize the catastrophe (rescue) frequencies as a function of the distance to the gold stripe for the strong dependence on MT length, each time interval a MT spent growing (shrinking) was multiplied by the catastrophe (rescue) frequency estimated for MTs of that length. This estimated frequency was obtained from a simple linear fit to the data shown in the middle panels of Fig. 10 in case of the catastrophe frequency and from a simple exponential fit to the data shown in the middle panels of Fig. 11 in case of the rescue frequencies. (Note that in principle these data would have to be corrected for the dependence on the distance to the gold stripe to obtain the true frequencies as a function of MT length; however, since the dependence on the distance is not very strong and averages were made over many MTs at all distances from the gold stripe, we assumed that the uncorrected data are a reasonable approximation to these true frequencies.) Summing the thus obtained values in each 5-μm-wide band gave the expected number of catastrophe (rescue) events in the absence of any distance dependence and dividing the actual number of observed events by this expected number of events gave the normalized distance dependence of the catastrophe (rescue) frequency.

Statistical Methods

Testing the Shift in Aster Anisotropy in the Presence of Chromatin. In Fig. 7 *a* standard Student's *t* test was used to show that the average aster anisotropy observed in mitotic extracts in the presence of chromatin is significantly different from the average anisotropy observed in the absence of chromatin. We find a significance α of 0.025. This significance gives the probability that the two data sets are drawn from distributions with identical means, i.e., it gives the probability that the average aster anisotropies are not different for the two cases.

Testing the Distance-to-Gold-Stripe Dependence of the Dynamic Parameters. To establish whether the catastrophe and rescue frequencies depend on the distance to the chromatin stripes in mitotic extracts, the hypothesis that they are in fact independent of this distance was tested. Using weighted least squares the normalized data (shown in the right panels of Figs. 10 and 11) were fitted to a constant function and then the quality of the fits obtained in the presence and absence of chromatin was compared. A measure for the quality of the fit can be obtained by calculating the chi-squared (χ^2) and associating a significance level α with the value obtained (which depends on n, the number of degrees of freedom of the fit, which is given by the number of data points minus the number of parameters used to obtain the fit). This significance level gives the probability to find a χ^2 as high or higher as the one obtained for a particular data set in case the hypothesis used to obtain the fit was correct (i.e., in the absence of any dependence on the distance to the gold stripe). For the catastrophe frequency we find a χ^2 of 22.4 (α = 0.004 for n = 8) in the presence of chromatin and a χ^2 of 8.9 (α = 0.4 for n = 8) in the absence of chromatin. This suggests that the hypothesis that the catastrophe frequency does not depend on the distance to the gold stripe is less likely to be true (by two orders of magnitude) in the presence of chromatin than in the absence of chromatin. For the rescue frequency we find respectively a χ^2 of 14.7 (α = 0.07 for n = 8) and a χ^2 of 9.0 (α = 0.3 for n = 7).

Errors and Limitations

Fluorescence Intensity. To estimate the anisotropy in aster structure, the

fluorescence intensity on opposite sides of the centrosome was integrated. This is an indirect way of measuring the amount of polymer nucleated by the centrosome, which has two important advantages: (a) it can be done automatically by the computer, which makes it fast; (b) it does not involve the identification of individual MTs by the (possibly biased) human eye. A few sources of error, however, exist. To distinguish signal produced by MTs from background fluorescence an appropriate cut-off in gray scale was chosen (by eye) and only pixels brighter than this cut-off were integrated. Thus, the actual number of pixels taken into account per MT is larger in areas where the background fluorescence is higher (such as very close to the centrosome). This number of pixels will also depend on how well each MT is in focus. Additional errors can result from the presence of small free MTs and uneven illumination. The asymmetry that we find for each individual aster is the result of a combination of real anisotropy in MT growth, fluctuations due to MT dynamics (that are not averaged out over the finite time interval during which we observe each aster) and the errors mentioned above. This leads to a distribution of anisotropies for asters measured under similar conditions. Only by measuring the anisotropy of many asters both in the presence and absence of chromatin, can we establish whether this distribution is biased in the direction of the chromatin (see Fig. 7).

Dynamic Parameters. The errors for the dynamic parameters that are shown in the plots are all statistical errors (as in Verde et al., 1992). As previously discussed (Verde et al., 1992) there are other sources of error in the estimation of the dynamic parameters that one should keep in mind. Statistical errors, however, dominate.

A point of concern is the variability we observe between different (identically prepared) samples and even between different asters in the same sample. When we present dynamic parameters as a function of distance to the chromatin stripes, one should keep in mind that several asters (from several samples) contribute to the results in each 5-μm-wide band, but that not all asters contribute to all bands (since the distance between the asters and the gold stripes varies). Therefore, some of the variation we find as a function of distance to the gold stripe may result from the way the asters are distributed over this distance (indicated in Fig. 7). We find variability to be especially large in the experiments with low-speed meiotic extracts and salmon sperm chromatin (see for example Fig. 3). Because of this, and because we cannot reproduce the same geometry of chromatin structure for each aster in these experiments, we only give results for individual asters. This has the disadvantage that the statistics on the dynamic parameters remain very limited. As a result we cannot, as we would like, measure parameters as a function of distance to the chromatin, but can at most compare the dynamics of MTs growing in the right direction with the dynamics of MTs growing in the wrong direction. By making only this very rough distinction, we may to some extent be averaging out the distance dependence we are interested in.
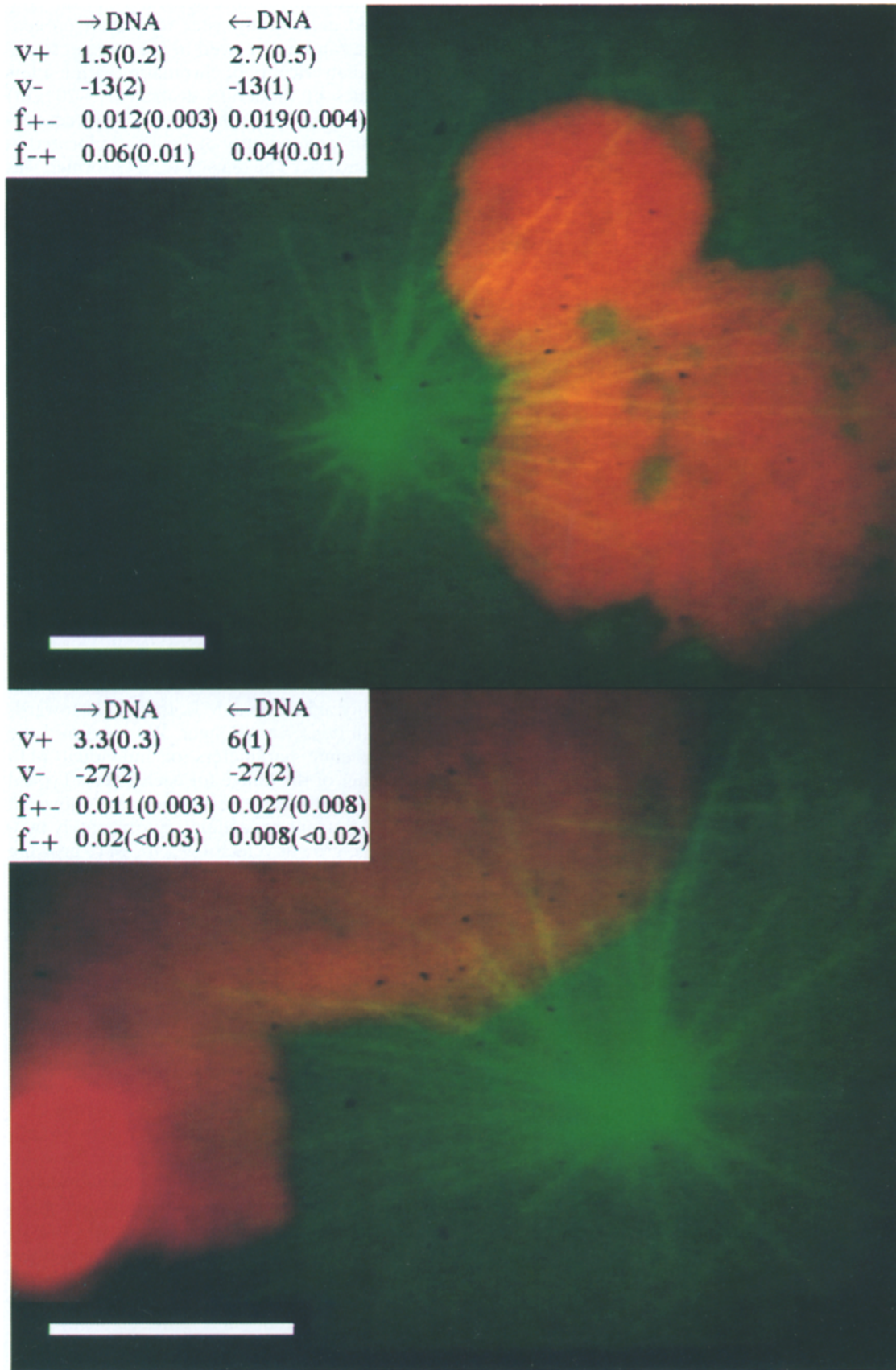
Results

Sperm Chromatin in Low-Speed Meiotic Extracts

Meiotic, low-speed extracts support spindle formation around *Xenopus laevis* sperm nuclei (Sawin and Mitchison, 1991). When fully developed, these spindles contain a large number of MTs nucleated by the centrosome initially associated with the nucleus. We were unable to find conditions that would reduce the number of MTs in these spindles and allow the measurement of the dynamics of individual MTs. We therefore used another source of chromatin: when highly condensed salmon sperm nuclei were introduced in these same extracts, they rapidly swelled in a similar way that is observed with *Xenopus* sperm nuclei. At low densities they subsequently formed condensed mitotic chromatin, fell into small pieces, and dispersed, but at the densities used in our experiments they stayed intact as large irregularly shaped clumps of chromatin. We assumed that in this case, as with *Xenopus* sperm under similar conditions, no kinetochores were present. In addition, no centrosomes were associated with these nuclei and no spindles formed.

We added purified centrosomes separately to this system which enabled us to study aster formation on centrosomes that were randomly placed in the sample, sometimes in the immediate vicinity of chromatin (within a few microns), sometimes at moderate distances (5–20 μm) away from the chromatin. (Note that we had no direct control of the geometry and quantity of chromatin located in the vicinity of MT asters.) The density of MTs formed was in general much lower than observed in fully developed spindles, which allowed us to measure the dynamic parameters of individual MTs. A possible reason for this lower density of MTs is that we added the salmon sperm nuclei at such large densities that they could not fully condense into mitotic chromatin. This useful reduction of MT density could not be obtained by increasing the density of *Xenopus* sperm nuclei, because each nucleus comes with a pair of associated centrioles. The increase in centrosome density led to the formation of multipolar spindles and aggregates, or, to the abrupt loss of MT polymerization, since the centrioles no longer formed active centrosomes in a reproducible way (Félix et al., 1994).

Stabilization of Microtubules in Close Contact with Chromatin. Fig. 3 shows two typical examples of MT asters nucleated from centrosomes placed in the immediate vicinity of salmon sperm chromatin. We assume that MTs come in close contact with the chromatin (and can be affected by short-range stabilization effects) when they appear superimposed with the DNA in our images. (Given the sample thickness this means that the distance is at most on the order of 2 μm.) It is clear even from these two snapshots that the asters are highly anisotropic: MTs that point towards chromatin are both denser and longer. We measured the values of the dynamic parameters of individual MTs (shown in the corner of the image for each aster). Typical traces of individual MT length versus time are shown in Fig. 4. We observe a strong reduction (approximately twofold) of the average growth velocity, v_+, for MTs growing in the direction of the chromatin. In contrast, the average shrinkage velocity, v_-, for these MTs remains unaffected. It seems that for MTs growing towards chromatin f_{+-} decreases (by ~50–100%) while f_{-+} increases. The effect on the frequencies of catastrophes and rescues is however harder to quantitate due to a small total number of events (see Materials and Methods). Also, one should keep in mind that the dynamic parameters of the MTs growing towards the chromatin are averaged over all MTs in that particular half of the aster. The growth velocity, for instance, varied in fact considerably between different MTs (see Fig. 4) and MTs in direct contact with the chromatin were often observed to grow only very slowly or even pause (which could in principle simply be due to a reduced accessibility of the tubulin). These considerations, in addition to the variability observed in these low-speed extracts, makes it impossible to infer absolute numbers for these parameters from the present assays. However, the relative behavior of the dynamic parameters for the MTs growing towards and away from chromatin is reproducible even on a semi-quantitative level. It seems that MTs in close contact with chromatin are stabilized due to a decrease in v_+ in combination with a decrease of f_{+-} and an increase of f_{-+}, which leads to a strong anisotropy of MT asters (i.e., longer and more MTs in the direction of the chromatin).

	→DNA	←DNA
V+	1.5(0.2)	2.7(0.5)
V-	-13(2)	-13(1)
f+-	0.012(0.003)	0.019(0.004)
f-+	0.06(0.01)	0.04(0.01)

	→DNA	←DNA
V+	3.3(0.3)	6(1)
V-	-27(2)	-27(2)
f+-	0.011(0.003)	0.027(0.008)
f-+	0.02(<0.03)	0.008(<0.02)

Figure 3. Anisotropic MT asters (*green*) in close contact with salmon sperm nuclei (*red*) in meiotic *Xenopus* egg extracts (the bright red object in the lower picture is a fluorescent latex bead). These examples show the effect of short-range stabilization on MTs that are in direct contact with the chromatin. In the corner of each picture, the average values of the dynamic parameters are shown as measured for all MTs growing towards the chromatin (*left*) and for all MTs growing in the opposite direction (*right*). Statistical errors are given between brackets. Colors are artificial. Bars, 10 μm.
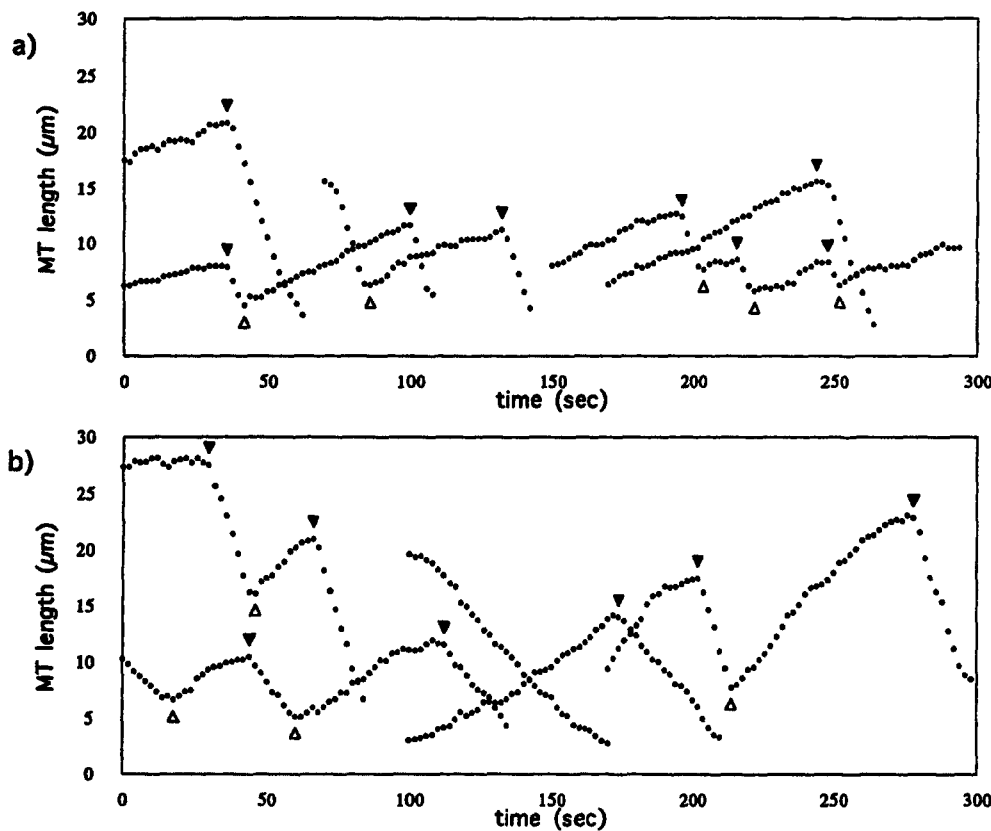
Figure 4. Examples of traces of MT length in low-speed meiotic (*a*) and high-speed mitotic (*b*) extracts. Catastrophe events are marked by closed arrows and rescue events are marked by open arrows.

Anisotropy of Microtubule Asters Distant From Chromatin. To test whether long-range guidance effects may also lead to the anisotropy of MT asters, we performed experiments in the same meiotic, low-speed extracts, however, with the centrosomes placed further apart from salmon sperm chromatin. Fig. 5 shows snapshots from five samples. It is important to stress that these samples are chosen at random so there is no bias as for the size or the shape of the asters, the chromatin, etc. (We have rejected only the video data that were impractical for quantitative measurements, as discussed in Materials and Methods.) For each of the samples we obtain a time average of the fluorescence intensity of rhodamine-labeled tubulin performed over times much larger than the turnover time of individual MTs. From this, we calculate the maximum asymmetry vector (see Fig. 2 and Materials and Methods) indicated by the arrows in Fig. 5. Although the direction of this vector varies from sample to sample, it is clear that it is biased towards the neighboring chromatin. We do not observe any case in which the aster is anisotropic with the asymmetry direction oriented away from the closest chromatin.

To verify the origin of this bias in anisotropy, we measured again the dynamic parameters of MT assembly (shown for each case in the upper left panel of Fig. 5). Despite some variability from sample to sample, we can conclude from these measurements that the velocities of growth and shrinkage are quite isotropic and independent on the position of the aster with respect to chromatin. It is the frequency of catastrophes, f_{+-}, which seems to be anisotropic: in four out of five cases analyzed here in detail, the MTs growing in the direction of the neighboring
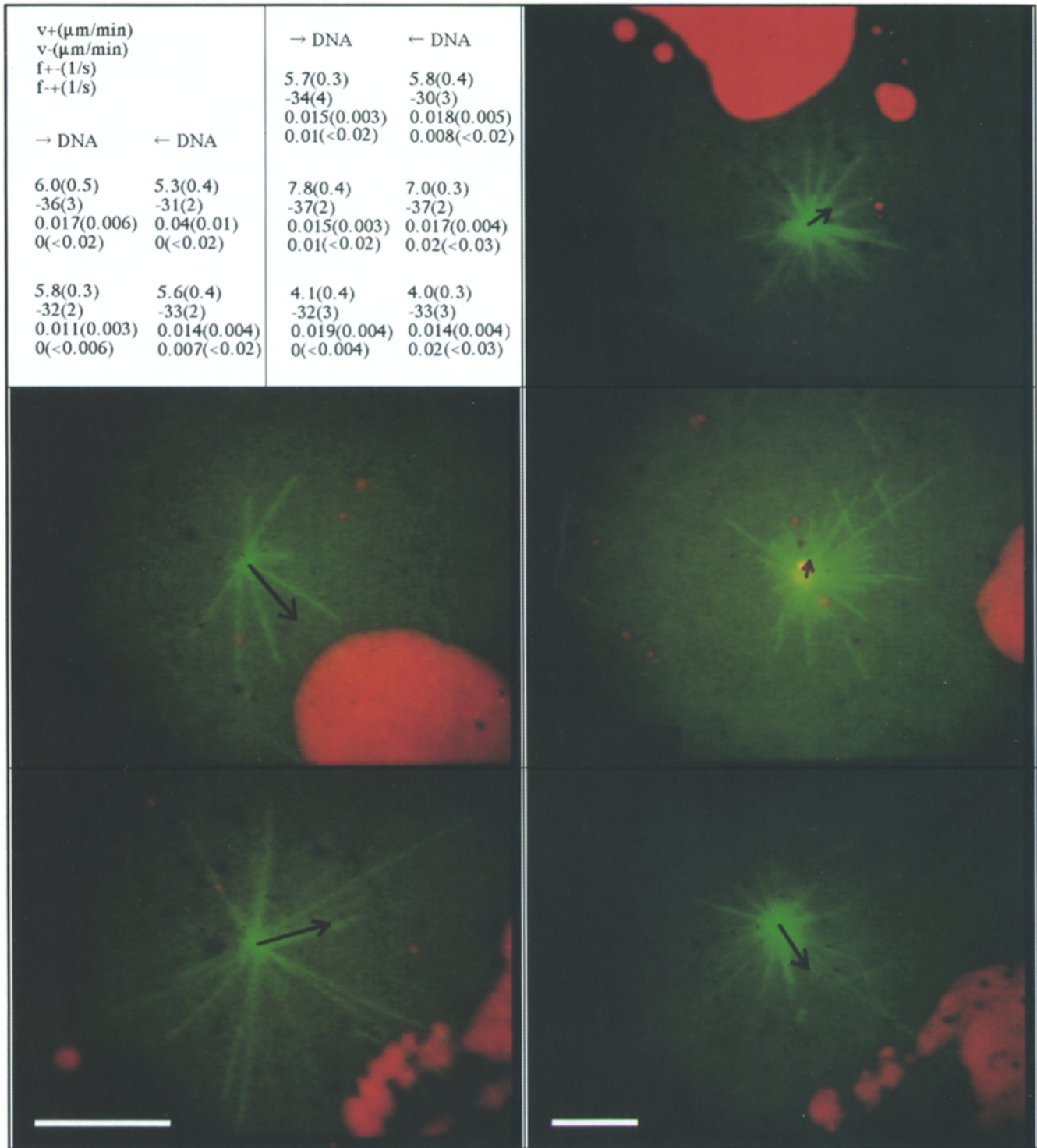
chromatin have the value of f_{+-} lower than those growing away from the chromatin. The rescue events being extremely rare, we cannot really gather any statistically significant values.

In conclusion, the measurements performed on MTs grown in meiotic extracts distant from chromatin, suggest the existence of a weak anisotropy of the asters induced by the presence of the chromatin. In contrast to the case of short-range stabilization, where the strong anisotropy of asters is due to changes in v_+, f_{-+} and f_{+-}, the source of the anisotropy here seems to be a long-range "guidance" effect which only affects the frequency of catastrophes, f_{+-}.

Chromatin Stripes in High-speed Mitotic Extracts

Construction of Artificial Chromatin Stripes. To obtain more statistically relevant results on the observed guidance effects we needed a better controlled system that would allow us to perform many times the same experiment under similar conditions. In the system described below we made several changes with respect to the first experiments in an effort to obtain the best possible reproducibility.

Mitotic, high-speed extracts from *Xenopus* eggs present several advantages for a quantitative analysis of MT assembly dynamics. For instance, they are much more homogeneous and therefore show much less variability than meiotic low-speed extracts. Furthermore, the use of Δ90 cyclin B allows one to reproducibly obtain stable mitotic-like extracts from high-speed supernatants. (Unfortunately, we failed to produce stable high-speed meiotic extracts that behaved in a similarly reproducible way.) If one

v+(μm/min) v-(μm/min) f+-(1/s) f-+(1/s)		→ DNA	← DNA
		5.7(0.3) -34(4) 0.015(0.003) 0.01(<0.02)	5.8(0.4) -30(3) 0.018(0.005) 0.008(<0.02)
→ DNA	← DNA		
6.0(0.5) -36(3) 0.017(0.006) 0(<0.02)	5.3(0.4) -31(2) 0.04(0.01) 0(<0.02)	7.8(0.4) -37(2) 0.015(0.003) 0.01(<0.02)	7.0(0.3) -37(2) 0.017(0.004) 0.02(<0.03)
5.8(0.3) -32(2) 0.011(0.003) 0(<0.006)	5.6(0.4) -33(2) 0.014(0.004) 0.007(<0.02)	4.1(0.4) -32(3) 0.019(0.004) 0(<0.004)	4.0(0.3) -33(3) 0.014(0.004) 0.02(<0.03)

Figure 5. Snapshots of MT asters and time-averaging of their anisotropy in the vicinity of salmon sperm nuclei in meiotic extracts. In the absence of direct contact between the MTs and the chromatin, long-range guidance effects lead to a weak anisotropy in aster structure. We integrated and time-averaged the fluorescence intensity produced by MTs on opposite sides of an axis that runs through the center of each aster (see Fig. 2). We varied the direction of this axis and drew an arrow perpendicular to the axis that maximizes the difference in fluorescence intensity. The strength of asymmetry is encoded in the length of the arrow: the amount by which the ratio in fluorescence intensity exceeds 1 is multiplied by 5 to give the arrow length in micrometers. The values of the dynamic parameters are summarized in the upper left panel: for MTs growing towards the chromatin (*left*) and for MTs growing in the opposite direction (*right*). Colors are artificial. Bars, 10 μm.

introduces free DNA molecules (like DNA from λ-phage) into mitotic extracts one observes condensation of the DNA that results in the formation of chromatin structures (Hirano and Mitchison, 1991). In general, the chromatin obtained in this way forms clumps of varying sizes and shapes. To control the geometry of chromatin structures, we specifically attached DNA molecules to gold stripes deposited onto the surface of a coverglass (Fig. 1 and Fig. 6, inset). The width of such stripes and their separation were much larger than the typical size of the MT asters. Thus, for an aster growing near an interface between a gold covered stripe and an uncovered stripe (Fig. 6), one can neglect the influence of other stripes. Of course, such an interface is not perfectly straight: with the patterning technique we used, one obtains spatial fluctuations of the order of a couple of microns. However, the homogeneity of the DNA coverage and the contrast between any two neighboring glass and gold surfaces were very good (see Fig. 6, inset).

The construction of artificial chromatin stripes allowed us to repeat quantitative measurements on the MT asters in a well-defined, reproducible geometry of neighboring chromatin and thus to acquire statistically significant data. As a control we performed similar measurements on MT asters placed near gold covered stripes that had no DNA attached to them. Any effects observed in the original experiments, but not in the control, thus have to be attributed to the presence of DNA and/or the molecules it binds in mitotic extracts. We did not attempt to narrow this down to one specific component.

Anisotropy of Microtubule Asters in Mitotic Extracts. The simplest measure of the anisotropy of MT asters is a global time-averaged analysis of the excess fluorescence in the direction of gold stripes (see Materials and Methods). We measured in this way the anisotropy for MT asters both in the presence (Fig. 7 a) and in the absence (Fig. 7 b) of chromatin. The anisotropy coefficient measuring the excess of fluorescence for individual asters varies substantially from aster to aster in both cases. This variability, which is probably due to some systematic errors in addition to variability of centrosomes and immunogenicities of the extracts (see Materials and Methods), is of comparable magnitude in both types of experiments. Due to such effects we do not observe any systematic dependence of aster anisotropy on the distance between its center and the neighboring gold stripe. However, the presence of chromatin introduces a statistically significant shift in the anisotropy distribution, a standard Student's t test comparing the two cases gives the significance coefficient $\alpha = 0.025$ (which is a very small value of the probability that the average aster anisotropy is the same in the two cases, see Materials and Methods). In addition, it is important to note, that we do not observe any cases of MT asters with anisotropy in the direction opposite to chromatin stripes (Fig. 7 a).

Measurement of the Dynamics of Microtubules Nucleated by Centrosomes. The direct measurement of the dynamic parameters for individual MTs is much more labor intensive than the global fluorescence anisotropy measurements. However, in contrast to the latter it is not sensitive to possible artifacts such as uneven background illumination, small number of free MTs, contribution from unpoly-

merized tubulin, etc. We therefore measured the dynamics of the assembly of individual MTs in all the asters analyzed above (Fig. 7) for their global anisotropy.

The dynamics of assembly, taking place at the tips of individual MTs, may in principle be influenced both by their distance to chromatin and their distance to the centrosome (i.e., the length of the MT itself). We thus kept track of both these variables while measuring the dynamic parameters (velocities and frequencies). In Fig. 8 we summarize all the counted dynamic events as well as their distribution around the centrosome. In the left panels we plot the position (x, y) with respect to the centrosome of each growth and shrinkage event (taken at 2-s intervals) both in the presence and absence of chromatin. In a similar way the positions of the catastrophe and rescue events are plotted in the middle and right panels, respectively. From these plots it is clear that the MTs we followed for the measurement of the dynamic parameters were evenly distributed around the centrosomes.

Velocities of Growth and Shrinkage of Microtubules. In Fig. 9 we represent the data on the velocities of growth and shrinkage of individual MTs. Since the velocities can be measured over every time interval in the entire period of an experiment, the obtained statistics are excellent (except for extremal points on these graphs, where obviously less MTs were analyzed, see Fig. 8). It can be clearly seen from the graphs that the velocities do not depend in any substantial way neither on the MT length nor on the distance to the chromatin.

An interesting issue is the fact that the observed velocity of growth, v_+, seems to be smaller in the presence of chromatin than in its absence, where we find values similar to our previous experiments in mitotic extracts (Verde et al., 1992). The shrinkage velocity, v_-, is the same in both cases.
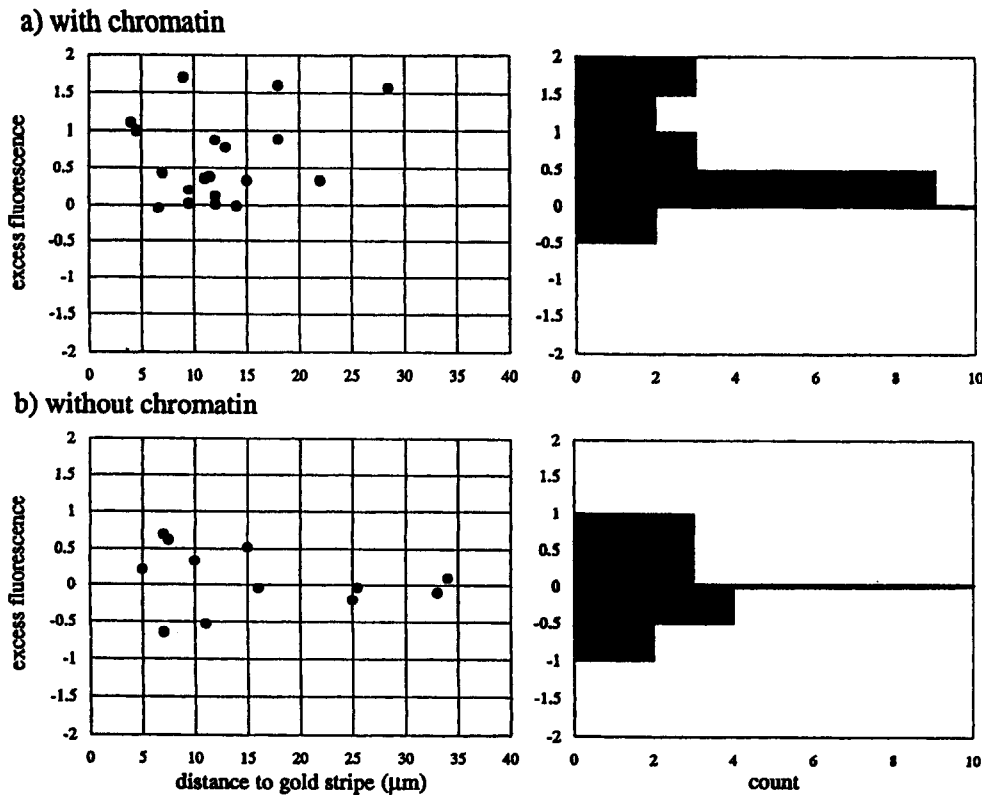
Frequency of Catastrophes and Rescues as a Function of the Length of Microtubules. First surprising conclusion from our measurements of MT dynamics is the observation that the frequencies of catastrophes and rescues depend on the MT length. The central panels of Figs. 10 and 11 clearly show that f_{+-} increases with the MT length, and f_{-+} decreases with the MT length. Each point on the graphs corresponds to an average over many MTs with the same length but pointing in different directions (see Fig. 8).

The length dependence of the catastrophe frequency is quite similar in both cases (chromatin present and absent on gold stripes). We expect that for a large enough number of MTs any potential effects of anisotropy in the presence of chromatin have been averaged out, but still may lead to a small difference with the results obtained in the absence of chromatin. The statistics for the rescue frequency are relatively poor—this may partially explain the difference of the obtained values for f_{-+} in the presence and in the absence of chromatin. However, the observed trend of decreasing f_{-+} with increasing MT length is the same in both cases.

The length dependence of the frequencies was not studied in previous analysis of MTs nucleated by centrosomes in mitotic extracts, such as those by Verde et al. (1992). The present study has increased substantially the statistics of the measurements (i.e., the total number of events, see Fig. 8), making such measurements possible.
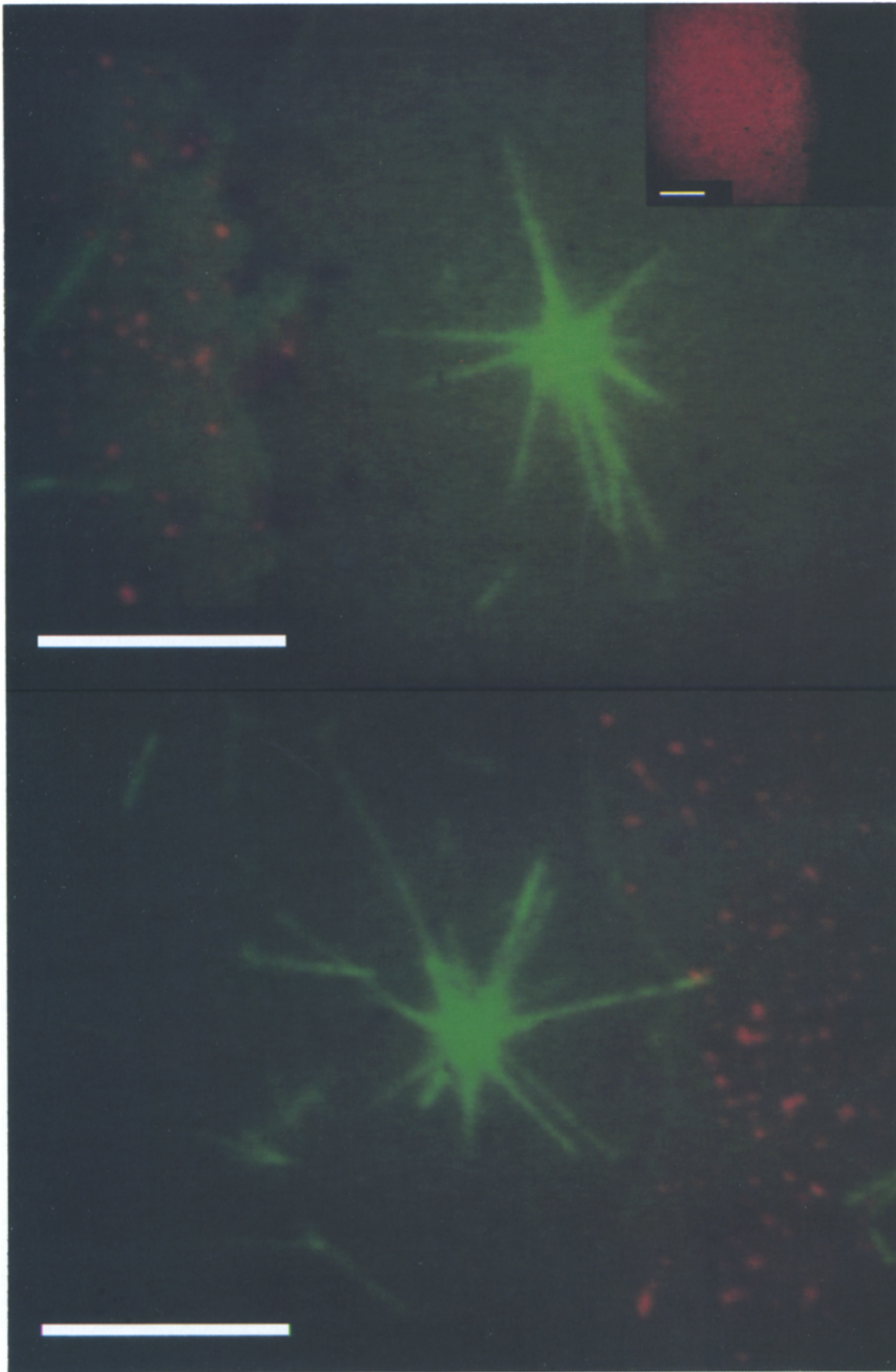
Figure 6. Examples of MT asters in the vicinity of chromatin stripes in mitotic extracts. Chromatin stripes were constructed by attaching λ-DNA molecules to gold stripes evaporated on glass coverslips. The inset shows the edge of such a stripe before incubation in the extract (DNA-coated gold on the left and uncoated glass on the right). Upon incubation in the extract the DNA assembles proteins and condenses into small chromatin-like structures. Colors are artificial. Bars, 10 μm.

a) with chromatin

b) without chromatin

distance to gold stripe (µm)

count

Frequency of Catastrophes and Rescues in the Presence of Chromatin. First panels of Figs. 10 and 11 show the frequencies of catastrophes and rescues measured in the presence (*a*) and absence (*b*) of chromatin as a function of the distance to the closest gold stripe. The larger dispersion of data in *b* is due to the smaller number of total events analyzed. To interpret these curves directly one has to take into account the strong length dependence of f_{+-} and f_{-+} discussed above. Indeed, two aster MTs undergoing a catastrophe or a rescue at the same distance from the chromatin stripe may have different lengths. For this reason we normalized the frequencies so as to take into account the lengths of MTs (see Materials and Methods). The results are represented in the third panels of Figs. 10 and 11.

We applied the χ^2 statistical test to these data to check whether the frequencies f_{+-} and f_{-+} can be considered independent on the distance to the closest gold stripe. For the catastrophe frequencies the χ^2 values are 22.4 for stripes covered with chromatin (the significance level being α = 0.004), and 8.9 for stripes with no chromatin (α = 0.4). The significance level gives the probability of obtaining a particular set of experimental data in the absence of any distance dependence. This shows that in the presence of chromatin it is unlikely that the distance dependence of f_{+-} is given by a constant. Fig. 10 suggests that f_{+-} is constant for distances larger than 15–20 µm (same as without chromatin) and monotonically decreases below these distances.

For the rescue frequencies the χ^2 values are 14.7 (α = 0.07) and 9.0 (α = 0.3), respectively. Thus, although it is still safe to say that the presence of chromatin might introduce some non-trivial dependence of f_{-+} on the distance of the MT tip to the chromatin stripe, the relatively poor statistics of our rescue data does not allow us to conclusively demonstrate (and describe) this dependence. Note that overall the values for f_{-+} seem to be higher in the presence of chromatin than in its absence (both in first and second panels).

Discussion

Establishment of Quantitative In Vitro Assays for Microtubule Dynamics in the Presence of Chromatin

In this study, we established quantitative assays for MT dynamics in the presence of chromatin. In general, the main difficulties associated with such assays are: (*a*) in the presence of chromatin the density of MTs is often very high and one cannot measure the dynamics of individual MTs. This problem was solved in both experiments described above; (*b*) the chromatin obtained from sperm nuclei or through the addition and condensation of free DNA forms very irregular patches, clumps, etc., making difficult any geometrical control of the assembly, which is essential for the study of long-range diffusive effects such as the guidance effects discussed in this paper. This problem was in addition solved in the second experiment described above. Also, we significantly increased the statistics of the measurements of MT dynamics as compared to past studies. As a consequence, we observed in mitotic extracts a non-trivial dependence of the frequencies of catastrophes and rescues on the MT length.
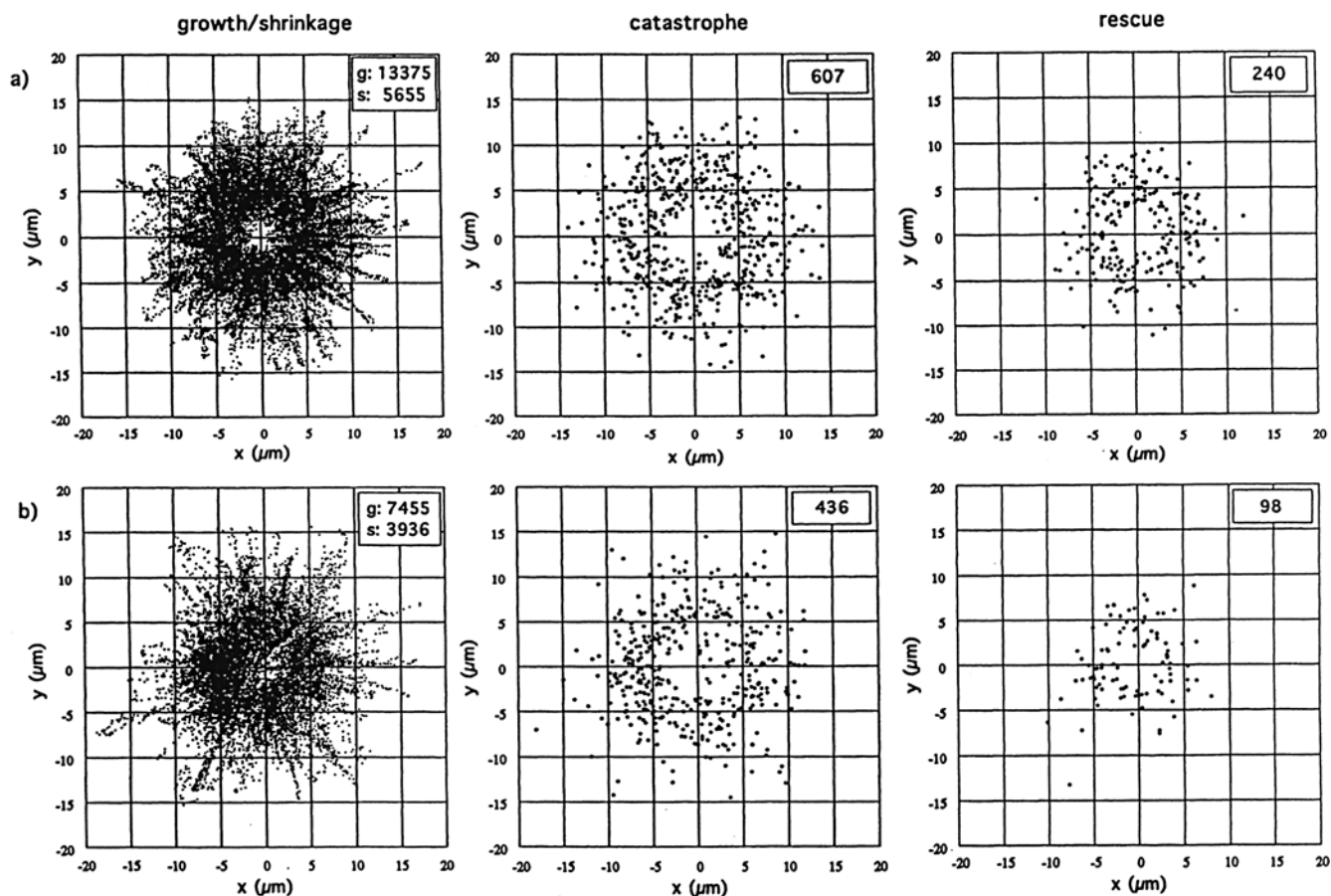
Figure 8. Spatial distribution around the centrosome of all dynamic events counted in the experiments with mitotic extracts and chromatin stripes. Shown are the positions (x, y) of the growth and shrinkage events (*left*), catastrophe events (*middle*) and rescue events (*right*) in the presence (*a*) and absence (*b*) of chromatin. All asters were rotated so that the gold stripe is located on the right, and the position of the centrosomes was superimposed (note that the distance to this stripe is different for each aster). The total number of events is shown in the upper right corner of each plot.

We consider, however, the present work only as a first step towards the quantitative in vitro control of the MT–chromatin interactions. In our opinion, particularly promising is the assay in which the condensed chromatin originates from DNA molecules attached to the prepatterned glass surface. This kind of assays may be extended in several directions: (*a*) higher DNA concentrations and different geometries may in principle be obtained through the appropriate control of chemistry on gold surfaces; (*b*) DNA including centromere sequences may be used to insure the formation of kinetochore-like structures (Sorger et al., 1994); (*c*) meiotic, low-speed extracts or other intermediate extracts may in principle be used in the same assays. This last point is of particular importance, since it may lead in the future to the isolation of molecular components responsible for the phenomena observed here through a systematic fractionation of the extracts.

Dynamic Assembly Parameters Depend on the MT Length

It was shown previously that in mitotic extracts the active cdk-cyclin B modifies the frequencies of catastrophes and rescues, inducing a drastic change in the structure of MT

asters nucleated around isolated centrosomes (Belmont et al., 1990; Verde et al., 1992). A simple mathematical model explained the connection between the measured dynamic parameters, the changes in aster structure, and the distribution of MT lengths (Verde et al., 1992).

In all previous studies it was implicitly assumed that the dynamic parameters do not depend on the instantaneous MT length. The increase of statistics in the present study allowed us to observe that, in contrast to the velocities of growth and shrinkage, the frequencies of catastrophe and rescues strongly depend on the distance between the MT tip and the centrosome. This unexpected result naturally leads to the following questions:

(*a*) What is a possible microscopic mechanism of this dependence? One general molecular scheme that can be imagined would be a diffusible factor originating at the centrosome and affecting the dynamics of MTs. Another probable explanation of the observed behavior is an accumulation of a destabilizing factor on the growing MTs or a progressive decrease in efficiency of a stabilizing factor, such as a microtubule-associated protein (MAP). A particularly attractive possibility is the one in which the destabilizing factor is simply the mechanical strain accumulating in a growing MT. Recent experiments for MTs assembled

136
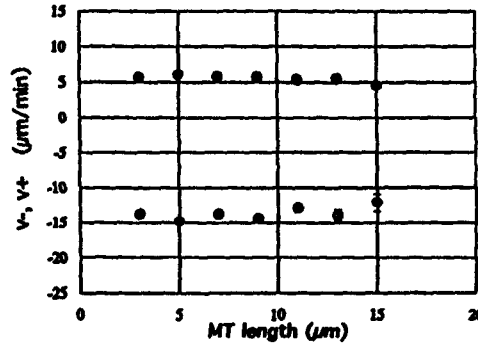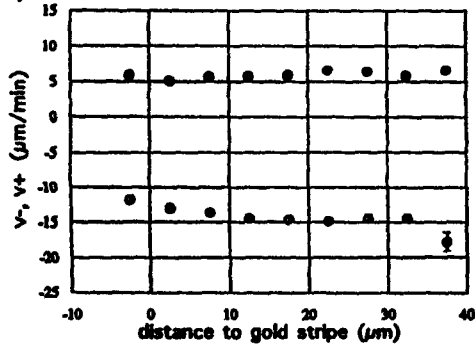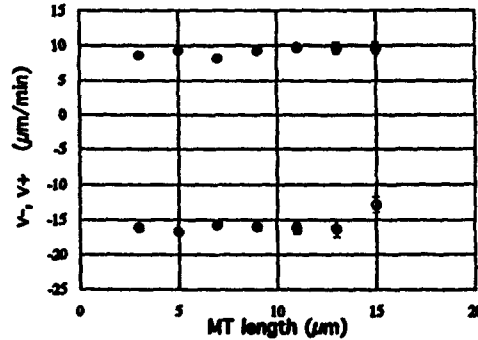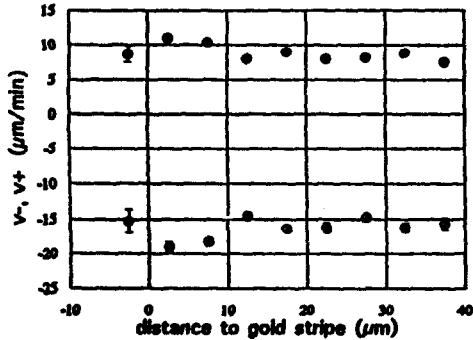
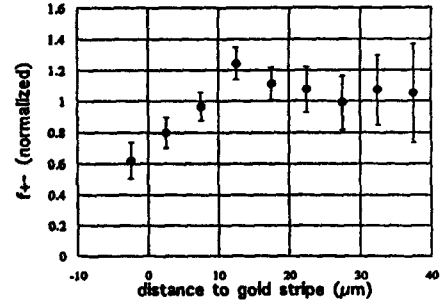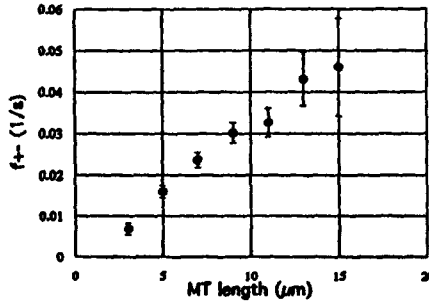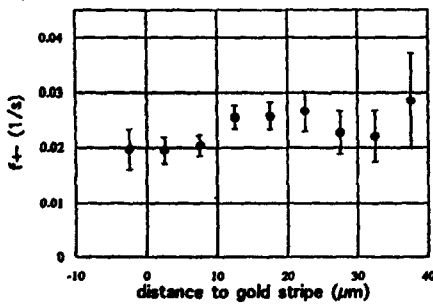## a) with chromatin

b) without chromatin

Figure 9. Average growth (*closed circles*) and shrinkage (*open circles*) velocities in the presence (*a*) and absence (*b*) of chromatin in mitotic extracts. (*Left*) As a function of distance to the gold stripe; (*right*) as a function of MT length. The error bars represent the standard errors in average velocities, not the spread (standard deviation) in velocities. The growth and shrinkage velocities do not depend on the distance to the chromatin, nor on the MT length.

in pure tubulin indeed suggested that the hydrolysis of GTP may induce conformational changes in tubulin protofilaments (Chretien et al., 1995) and thus introduce mechanical strains, which eventually lead to a rapid, collective depolymerization. Of course, one has to be cautious in using these results to explain our observations because of the presence of MAPs in the mitotic extracts. In pure tubulin, the length dependence of the dynamic pa-

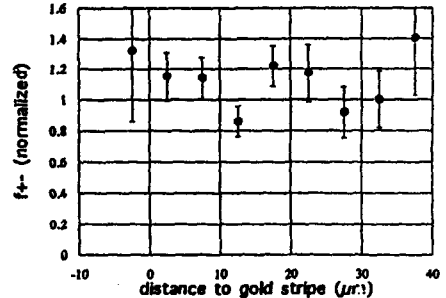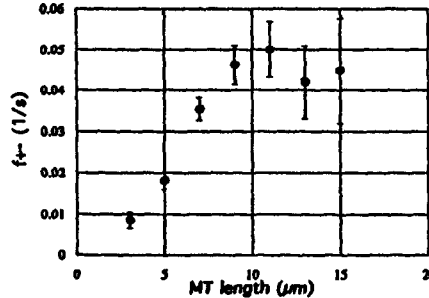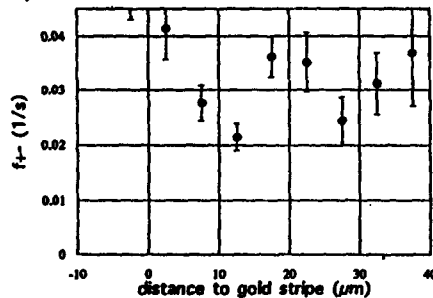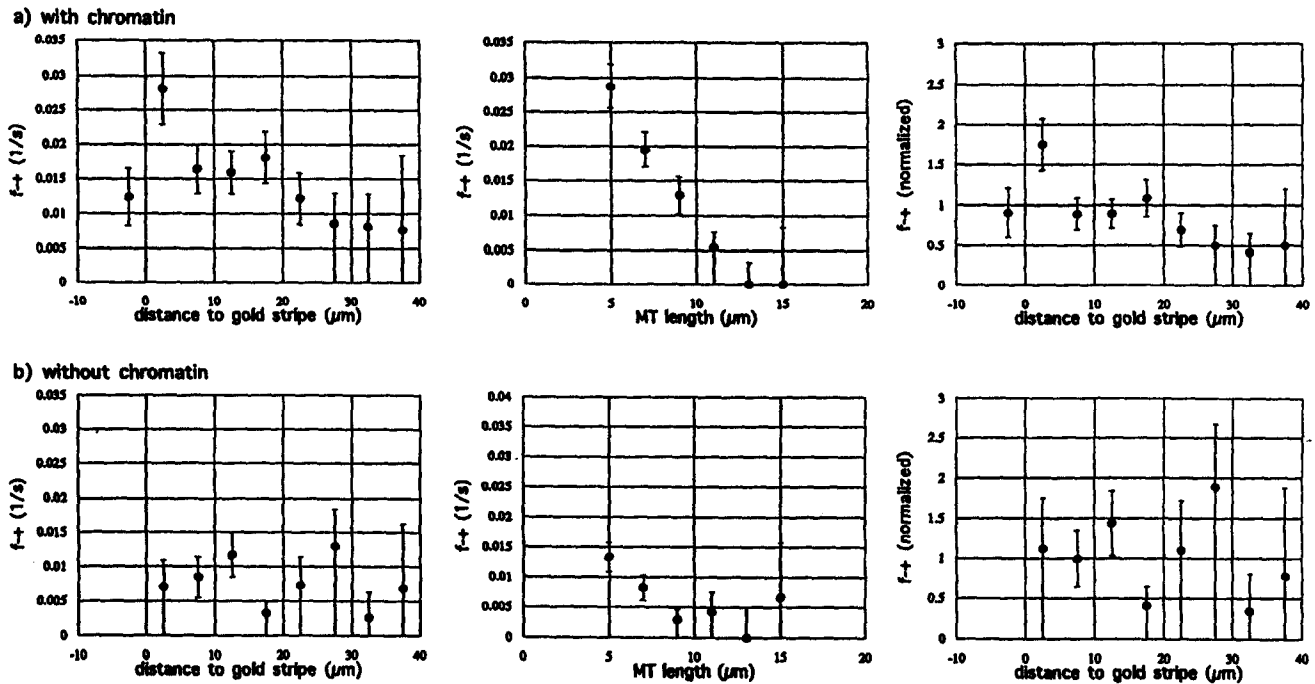## a) with chromatin

b) without chromatin

Figure 10. Catastrophe frequency in the presence (*a*) and absence (*b*) of chromatin in mitotic extracts. (*Left*) As a function of distance to the gold stripe; (*middle*) as a function of MT length; (*right*) normalized frequency as a function of distance to the gold stripe (corrected for the MT length dependence). The error bars represent statistical errors due to a limited number of observed events. In the presence of chromatin the normalized catastrophe frequency decreases close to the gold stripe, while in the absence of chromatin it does not. In both cases, the catastrophe frequency increases strongly with MT length.

Figure 11. Rescue frequency in the presence (*a*) and absence (*b*) of chromatin in mitotic extracts. (*Left*) As a function of distance to the gold stripe; (*middle*) as a function of MT length; (*right*) normalized frequency as a function of distance to the gold stripe (corrected for the MT-length dependence). Note that whenever fewer than seven rescue events were observed, an upper bound to the rescue frequency is given. The error bars represent statistical errors due to a limited number of observed events. The rescue frequency decreases strongly with MT length. The normalized rescue frequency does not significantly depend on the distance to the chromatin.

rameters for MTs has been studied by analyzing the distribution of growth times for MTs nucleated by axonemes (Odde et al., 1995). In this case the relative small number of short growth times led to the conclusion that the catastrophe frequency depends on MT length. We cannot make a direct comparison between the two data sets since a plot of the distribution of growth times as given by Odde et al. (1995) requires conditions under which very short MTs can be followed as unambiguously as long ones. Surely in our experiments (and possibly also in the pure tubulin case) it is harder to follow short MTs due to the high fluorescence intensity close to the centrosome and simply the limited resolution of optical microscopy.

(*b*) How does the observed length dependence of the frequencies of rescues and catastrophes affect the quantitative description of the structure of MT asters? To estimate to what extent the length dependence observed here changes the prediction of experimentally observed MT length distributions, such as those described in our earlier work (Verde et al., 1992), we compared the two cases in a simulation. We found that within the experimental resolution the differences in the predicted MT length distributions are smaller than typical statistical fluctuations (data not shown).

Strong Microtubule Asters Anisotropy in Meiotic (Low-Speed) Extracts Due to Short-Range Stabilization Effects

In our experiments with meiotic extracts we observed changes in MT dynamics leading to the formation of highly anisotropic asters when centrosome-nucleated MTs came close to chromatin from salmon sperm nuclei. One should note that the anisotropy of the asters may also be reinforced by an (induced) anisotropic nucleation of MTs on the centrosome (as proposed in Rieder et al., 1993), resulting in a higher density of MTs growing towards chromatin. However, since the number of MTs is affected by many parameters simultaneously (MT growth dynamics, the density of nucleation sites, the nucleation rate, tubulin diffusion (Dogterom et al., 1995), this effect would be difficult to measure separately in the present assay.

The fact that we do not observe a similar strong short-range stabilization effect in our experiments with high-speed extracts, driven into a mitotic state by the addition of sea urchin Δ90 cyclin B, may be due to one or several of the following reasons: (*a*) it is possible that the MT-organizing role of chromosomes is more important in meiotic systems than in mitotic systems and that the stabilizing effect on MTs is stronger. This idea could be correlated with the fact that in many meiotic (but not mitotic) systems, spindle formation can occur in the absence of MT organizing centers such as the centrosome (Nicklas, 1988); (*b*) the source, density, and geometry of the chromatin used in the two extracts is very different. In particular, the artificially constructed chromatin stripes are thin, quasi-two-dimensional structures that may not be able to stabilize MTs through physical contact the way the salmon sperm chromatin can. Also, the surface density of DNA on the gold stripes may simply be too low; (*c*) the differences may be due to the difference between high- and low-speed extracts. The observed short-range stabilization effects may

require the presence of certain cytoplasmic components, that are present in low-speed extracts, but not in high-speed extracts.

Long-Range Guidance of Microtubules towards Chromatin: Theoretical Considerations

In addition to short-range stabilization effects, we explored here the possibility that MT growth is guided towards chromatin during the search for chromosomes. During the initial stages of mitosis the parameters of dynamic instability seem to be optimized to find chromosomes in an efficient, although random, way (Holy and Leibler, 1994). The capturing of chromosomes would be even more effective if this random search was biased in the direction of the chromosomes. For instance, it was proposed (Karsenti, 1991; Karsenti et al., 1991) that a phosphatase localized on the chromatin (Fernandez et al., 1992) may act in opposition to the cyclin dependent kinase(s) active in mitosis. In such a case, a diffusible substrate for these enzymes could form a nonhomogeneous spatial distribution (a gradient) of its phosphorylation state (Dogterom, 1994; Dogterom, M., E. Karsenti, and S. Leibler, manuscript in preparation), and thus of its activity, which is the modification of the frequencies of the dynamic instability of MTs (Belmont et al., 1990; Verde et al., 1992). This in turn would induce an anisotropic steady-state length and number distribution of the MTs and decrease the time required to find the targets such as kinetochores.

This possibility would provide an example of how morphological information can be established in the cell and would suggest a general mechanism for the spatial regulation of cellular events. In fact, one can estimate that given the kinetics of typical enzymatic reactions and the diffusion properties of proteins it is possible for the cell to maintain gradients in enzymatic activity over typical cellular length scales (Dogterom, M., E. Karsenti, and S. Leibler, manuscript in preparation).

Weak Long-Range Guidance Effects Observed Both in Meiotic (Low-Speed) and Mitotic (High-Speed) Extracts

Both in meiotic and mitotic extracts we found evidence for the existence of the above discussed guidance effects in situations where MTs are not stabilized by close contact with the chromatin. We observed a decrease in catastrophe frequency in the vicinity of chromatin expected to lead to an increase in average MT length and MT density in the direction of chromatin that is consistent with the observed anisotropy in aster fluorescence intensity (Dogterom, M., E. Karsenti, and S. Leibler, manuscript in preparation). One should note that the apparently weak effects observed may be due to the experimental conditions chosen. Indeed, we purposely chose conditions that do not favor MT growth towards chromatin as much as under normal conditions to be able to observe individual MTs. Therefore, the effect observed may well be an underestimate of the actual effect that chromatin may have on MT growth.

Our experiments did not in any way address questions about the microscopic mechanisms responsible for the observed effects. As discussed before, one possibility would be that an active phosphatase associates with mitotic chromatin and counteracts the MT-destabilizing effect of the

cdc2 kinase. In our present assay we did not attempt to characterize the molecular composition of the chromatin structures. In a search for the molecular basis of the observed phenomena one could in principle, however, use similar quantitative experiments. One could for instance bind candidate phosphatases or intermediates directly to prepatterned surfaces and study quantitatively their effect on MT dynamics.

References

Belmont, L.D., A.A. Hyman, K.E. Sawin, and T.J. Mitchison. 1990. Real-time visualization of cell cycle-dependent changes in microtubule dynamics in cytoplasmic extracts. *Cell.* 62: 579–589.

Chretien, D., S.D. Fuller, and E. Karsenti. 1995. Structure of growing microtubule ends: two-dimensional sheets close into tubes at variable rates. *J. Cell Biol.* 129:1311–1328.

Church, K., R.B. Nicklas, and H.P. Lin. 1986. Micromanipulated bivalents can trigger mini-spindle formation in *Drosophila melanogaster* spermatocyte cytoplasm. *J. Cell Biol.* 93:2765–2773.

Dogterom, M. 1994. Physical aspects of microtubule growth and mitotic spindle formation. Ph.D. thesis. University of Paris-Sud. 178 pp.

Dogterom, M., A. C. Maggs, and S. Leibler. 1995. Diffusion and formation of microtubule asters: physical processes versus biochemical regulation. *Proc. Natl. Acad. Sci. USA.* 92:6683–6688.

Félix, M.-A., C. Antony, M. Wright, and B. Maro. 1994. Centrosome assembly in vitro: role of γ-tubulin recruitment in *Xenopus* sperm aster formation. *J. Cell Biol.* 124:19–31.

Félix, M.-A., J. Pines, T. Hunt, and E. Karsenti. 1989. A post-ribosomal supernatant from activated *Xenopus* eggs that displays post-translationally regulated oscillation of its cdc2+ mitotic kinase activity. *EMBO (Eur. Mol. Biol. Organ.) J.* 8:3059–3069.

Fernandez, A., D.L. Brautigan, and N.J.C. Lamb. 1992. Protein phosphatase type 1 in mammalian cell mitosis: chromosomal localization and involvement in mitotic exit. *J. Cell Biol.* 116:1421–1430.

Gard, D., and M. Kirschner. 1987. Microtubule assembly in cytoplasmic extracts of *Xenopus* oocytes and eggs. *J. Cell Biol.* 105:2191–2201.

Glotzer, M., A.W. Murray, and M.W. Kirschner. 1991. Cyclin is degraded by the ubiquitin pathway. *Nature (Lond.).* 349:132–138.

Hirano, T., and T.J. Mitchison. 1991. Cell cycle control of higher-order chromatin assembly around naked DNA in vitro. *J. Cell Biol.* 115:1479–1489.

Holy, T. E., and S. Leibler. 1994. Dynamic instability of microtubules as an efficient way to search in space. *Proc. Natl. Acad. Sci. USA.* 91:5682–5685.

Hyman, A., D. Drechsel, D. Kellogg, S. Salser, K. Sawin, P. Steffen, L. Wordeman, and T. Mitchison. 1991. Preparation of modified tubulins. *Methods Enzymol.* 196:478–485.

Karsenti, E. 1991. Mitotic spindle morphogenesis in animal cells. *Semin. Cell Biol.* 2:251–260.

Karsenti, E., J. Newport, and M. Kirschner. 1984. The respective roles of centrosomes and chromatin in the conversion of microtubule arrays from interphase to metaphase. *J. Cell Biol.* 99:47s–54s.

Karsenti, E., F. Verde, and M.A. Félix. 1991. Role of type 1 and type 2A protein phosphatases in the cell cycle. *Adv. Prot. Phosph.* 6:453–482.

Kirschner, M., and T. Mitchison. 1986. Beyond self-assembly: from microtubules to morphogenesis. *Cell.* 45:329–342.

Lohka, M.J., and Y. Masui. 1983. Formation in vitro of sperm pronuclei and mitotic chromosomes induced by amphibian ooplasmic components. *Science (Wash. DC).* 220:719–721.

McIntosh, J.R., and M.P. Koonce. 1989. Mitosis. *Science (Wash. DC).* 246:622–628.

Mitchison, T., and M. Kirschner. 1984a. Dynamic instability of microtubule growth. *Nature (Lond.).* 312:237–242.

Mitchison, T., and M. Kirschner. 1984b. Microtubule assembly nucleated by isolated centrosomes. *Nature (Lond.).* 312:232–237.

Mitchison, T.J., and M.W. Kirschner. 1986. Isolation of mammalian cen-
trosomes. *Methods Enzymol.* 134:261–268.

Murray, A. 1991. *Xenopus laevis:* Practical Uses in Cell and Molecular Biology.
B.K. Kay and H.B. Peng, editors. Academic Press, San Diego. 581–605.

Murray, A., and T. Hunt. 1993. The Cell Cycle: an Introduction. W.H. Free-
man, NY. 251 pp.

Nicklas, R.B. 1988. Chromosome Structure and Function: the Impact of New
Concepts. J.P. Gustafson and R. Appels, editors. Plenum Press, NY. 53–74.

Odde, D.J., L. Cassimeris, and H.M. Buettner. 1995. Kinetics of microtubule ca-
tastrophe assessed by probabilistic analysis. *Biophys. J.* 69:796–802.

Pickett-Heaps, J.D., D.H. Tippit, and K.R. Porter. 1982. Rethinking mitosis.
Cell. 29:729–744.

Rieder, C.L., J.G. Ault, U. Eichenlaub-Ritter, and G. Sluder. 1993. Chromo-
some segregation and aneuploidy. B.K. Vig, editor. Springer-Verlag, Berlin,
Heidelberg. 183–197.

Sawin, K.E., and T.J. Mitchison. 1991. Mitotic spindle assembly by two different
pathways in vitro. *J. Cell Biol.* 112:925–940.

Sorger, P.K., F.F. Severin, and A.A. Hyman. 1994. Factors required for the
binding of reassembled yeast kinetochores to microtubules in vitro. *J. Cell*

Biol. 127:995–1008.

Steffen, W., H. Fuge, P. Dietz, M. Bastmeyer, and G. Müller. 1986. Aster-free
spindle poles in insect spermatocytes: evidence for chromosome-induced
spindle formation? *J. Cell Biol.* 102:1679–1687.

Theurkauf, W.E., and R.S. Hawley. 1992. Meiotic spindle assembly in *Dro-
sophila* females: behavior of nonexchange chromosomes and the effects of
mutations in the nod kinesin-like protein. *J. Cell Biol.* 116:1167–1180.

Verde, F., J.C. Labbé, M. Dorée, and E. Karsenti. 1990. Regulation of microtu-
bule dynamics by cdc2 protein kinase in cell-free extracts of *Xenopus* eggs.
Nature (Lond.). 343:233–238.

Verde, F., M. Dogterom, E. Stelzer, E. Karsenti, and S. Leibler. 1992. Control
of microtubule dynamics and length by cyclin A and cyclin B dependent ki-
nases in *Xenopus* egg extracts. *J. Cell Biol.* 118:1097–1108.

Zhang, D., and R.B. Nicklas. 1995. The impact of chromosomes and cen-
trosomes on spindle assembly as observed in living cells. *J. Cell Biol.* 129:
1287–1300.

Zimmermann, R.M., and E.C. Cox. 1993. DNA stretching on functionalized
gold surfaces. *Nucleic Acids Res.* 22:492–497.